Research article

Novel inhaled andrographolide for treatment of lung cancer: *In vitro* assessment

Shankar Jothi [a], Noratiqah Mohtar [a], Mas Jaffri Masarudin [b], Thaigarajan Parumasivam [a,*]

[a] *School of Pharmaceutical Sciences, Universiti Sains Malaysia, 11800, Penang, Malaysia*
[b] *Faculty of Biotechnology and Biomolecular Sciences, Universiti Putra Malaysia, 43400, Serdang, Selangor, Malaysia*

ARTICLE INFO

ABSTRACT

Andrographolide is a plant-based compound that showed promising activity against lung cancer. However, the compound's poor water solubility and low bioavailability limit its oral administration. Inhaled drug delivery of andrographolide is highly favourable as it delivers active ingredients directly into the affected lungs. In the current study, we compared *in vitro* aerosol performance, anti-cancer activity and storages stability of two (2) inhalable andrographolide formulations. Formulation 1 was prepared using precipitation and spray drying techniques, while Formulation 2 was prepared via direct spray drying technique. Drug morphology and physico-chemical properties were confirmed using scanning electron microscopy (SEM) and X-ray diffraction (XRD) analysis. *In vitro* aerosol dispersion profile was evaluated using the next-generation impactor (NGI). Formulation 1 consisted of elongated crystals while Formulation 2 was made up of amorphous spherical particles. Both formulations had an inhalable fraction (<5 μm) of more than 40 %, making them suitable for pulmonary drug delivery. The formulations also showed an IC_{25} of less than 100 μg/mL against the human lung carcinoma cells (A549). Formulation 1 and 2 was stable in a vacuum condition at 30 °C for up to 6 and 3 months, respectively. Novel inhalable andrographolide dry powders were successfully produced with a good aerosol profile, potent anti-cancer activity and adequate storage stability, which deserve further *in vivo* investigations.

1. Introduction

Lung cancer is a malignant neoplasm that arises from the cells of the lung tissue. It is one of the most prevalent and deadly types of cancer globally, accounting for a significant number of cancer-related deaths. There were more than 2.2 million new cases of lung cancer worldwide in 2020. There are two main types of lung cancer: non-small cell lung cancer (NSCLC) and small cell lung cancer (SCLC). NSCLC is the most common type and accounts for about 85 % of all cases, while SCLC accounts for the remaining 15 % [1]. Lung cancer treatments include surgery, radiofrequency ablation, radiation therapy, chemotherapy, targeted drug therapy and immunotherapy. Surgery is the primary treatment for patients with early-stage cancer who are in good general health, while radiation therapy (radiotherapy) uses high-energy X-rays to destroy cancer cells [1]. Chemotherapy uses drugs that kill cancer cells and patients usually receive chemotherapy by direct injection into a vein or through a catheter placed in a large vein. The drawbacks of surgery for

---

lung cancer may include risks associated with general anaesthesia, pain, bleeding, infection, and a long recovery period. Surgery may not be an option for some patients, particularly those with advanced or metastatic lung cancer. While radiation therapy can be effective in treating lung cancer, it can cause side effects such as fatigue, skin irritation, difficulty swallowing, and damage to healthy tissue in the lung or nearby organs. Chemotherapy can cause many side effects, including nausea, vomiting, hair loss, fatigue, and an increased risk of infection. It can also have a negative impact on the quality of life for some patients [2].

Andrographis paniculata, commonly known as "Andrographis" or "King of Bitters," is a medicinal plant that has been used for centuries in traditional medicine systems, particularly in Ayurveda, Traditional Chinese Medicine (TCM), and other Southeast Asian traditional healing practices. It is native to South Asian countries like India, Sri Lanka, and Pakistan, as well as certain parts of Southeast Asia. *A. paniculata* is known for its bioactive components, particularly andrographolide, which has been extensively studied for its medicinal properties. Andrographolide has been identified as a major compound in the plant. Various studies have shown that andrographolide has a potential anti-cancer activity and has also shown to induce a programmed cell death (apoptosis) in several types of cancer cells, including lung cancer [3]. Studies have suggested that andrographolide may induce apoptosis by activating various signalling pathways, including the p53 pathway and the caspase pathway [4]. Additionally, andrographolide has been shown to inhibit the growth and proliferation of cancer cells by inducing cell cycle arrest, suppressing angiogenesis, and inhibiting cancer cell invasion and metastasis [5]. It also has been shown to inhibit the growth of cancer cells by interfering with cell signalling pathways involved in cell proliferation and survival [6]. However, andrographolide has a few drawbacks when administered orally. Its low oral bioavailability allows only a small fraction of the administered dose to reach the systemic circulation and cancer-affected area, limiting its therapeutic efficacy [7]. Oral andrographolide also has a short half-life due to its rapid metabolism and elimination from the body [8]. This may require frequent dosing to maintain the therapeutic concentrations. Oral administration of andrographolide also has been reported to cause gastrointestinal disturbances, such as diarrhea and nausea in some individuals [8,9]. It may interact with certain medications, such as blood thinners and immunosuppressants, which may affect their efficacy or toxicity [10,11].

We hypothesised that the administration of andrographolide via inhalation would overcome these drawbacks related to oral route for the treatment of lung cancer. First, the susceptibility of the medicine to degrade in the stomach's acidic environment is minimised by the targeted delivery to the lungs, which bypasses the initial metabolism. Studies have shown that andrographolide can undergo hydrolytic degradation in strong acidic conditions, such as low pH values (pH 1–3) or in the presence of hydrochloric acid (HCl) which can lead to the formation of different degradation products [12,13]. Second, the deposition of medicine in the pulmonary regions allows high drug concentration in the lungs, which can reduce the requirement for frequent dosing. Third, the pulmonary provides a large surface area for the rapid absorption of andrographolide into the bloodstream. Hence, inhalation therapy of andrographolide may enable a more effective treatment for lung cancer.

In the development of inhalable powders, spray drying has been heavily utilised to engineer powder formulations with suitable aerosol characteristics. Spray drying is a single-step manufacturing technique for drying a suspension or solution into dry powders using a rapid drying gas. It has the capacity for precise control over particle size and morphology for inhalation, as well as its suitability for large-scale and rapid production [14]. These characteristics render spray drying a preferred method for developing inhalable pharmaceuticals for respiratory drug delivery systems.

In the present study, we have produced two (2) dry powder formulations: (i) Formulation 1 - Andrographolide was precipitated into microcrystals and spray dried into inhalable particles, and (ii) Formulation 2 inhalable amorphous particles were produced through a direct spray drying of andrographolide in a co-solvent system. These two formulations were investigated for their physiochemical properties, *in vitro* aerosol performance and storage stability, as well as their *in vitro* anti-cancer activity.

2. Materials, chemicals and methodology

2.1. Materials

Raw andrographolide powder was procured from Xi'an Tian Guangyuan Biotech Co., Ltd, China. Analytical and HPLC grade solvents such as acetonitrile, ethanol and methanol were obtained from Fisher Scientific (United Kingdom). Phosphate Buffered Saline (PBS) tablets were purchased from Sigma Aldrich, Castle Hill, Australia. Tween 80 (polysorbate 80, polyoxyethylene sorbitan mon-ooleate) was purchased from Biolabs (USA) and potassium bromide (Kbr) was obtained from Fischer Scientific (New Hampshire, United States). Hydroxypropyl Methylcellulose (HPMC) clear type capsule size 3 was purchased from Alice Li's Pharmaceutical, China. Cellulose filter paper (Whatman® qualitative filter paper Grade 5) was procured from Fisher Scientific (New Hampshire, United States).

2.2. Cell culture

Adenocarcinomic human alveolar basal epithelial cells (A549 cells) were obtained from ATCC (Manassas, VA). The cells were cultured in RPMI growth media supplemented with 10 % FBS, 2 mM glutamine and 100 U/ml penicillin–streptomycin. Cells were maintained at 37 °C in a humidified atmosphere of 5 % CO_2.

2.3. Preparation of andrographolide dry powder

2.3.1. Formulation 1
100 mg andrographolide powder was dissolved in 30 mL ethanol absolute (99.7 %) and stirred until all powder was fully dissolved.

Then 20 mL distilled water was added to the solution and stirred until homogenous. The solution was subjected to evaporation under stirring at 60 °C until all ethanol was evaporated. The formed suspension solution was subsequently homogenised at 24 000 rpm for 2 min using homogeniser (Ultra Turrax T 25 Basic, IKA, Germany).

The aqueous suspension was then spray dried into a powder using a Mini Spray Dryer operated in open-loop connected with a Buchi-296 dehumidifier (B-290, Büchi Labortechnik AG, Switzerland) at the following parameters: Inlet temperature of 60 °C, atomiser at 60 mm (approximately 740 L/h), aspirator at 100 % (40 m^3/h), and feed rate of 2 mL/min. The dried powder was collected and kept in a desiccator until further analysis.

2.3.2. Formulation 2

100 mg andrographolide powder was dissolved in 20%v/v ethanol in water and subjected to spray drying using the Mini Spray Dryer with the same parameters as in Formulation 1. The dried powder was collected and kept in a desiccator until further analysis.

2.4. Characterisation of the formulations

2.4.1. Scanning electron microscopy (SEM)

Particle morphology was examined using Scanning Electron Microscope (Quant 650 FEG, (Thermo Fisher Scientific, United states)), equipped with Oxford Instruments (United Kingdom) X-MaxN 150 mm energy dispersive x-ray detector, at a 2500 V acceleration voltage. Powders were deposited onto carbon tape (aluminium substrate 8 mm × 20 M) and sputter coated with 15 nm of platinum using a K550X sputter coater (Quorum Emitech, UK) prior to the scanning.

2.4.2. Nuclear magnetic resonance (^{1}H NMR and ^{13}C NMR analysis)

5 mg of powder was mixed with 700 μL dimethyl sulfoxide-d6 (DMSO-D6) and sonicated for 15 min. The solution was placed in an NMR tube of 5 mm in diameter. An Avance III HD 700 NMR Spectometer (Bruker Ltd, Germany) was used to perform the analysis on the sample. The acquisition of the NMR spectra was carried out with the field strength set to 700 MHz, the relaxation delay set to 2.32 s, and the X offset fixed to 5.0 ppm. Each spectrum was collected over a period of 5 min with an acquisition of 128 scans and 12 parts per million. Analysis of 1^H and 13^C NMR spectra was performed with TopSpin® 3.6.2 software (Bruker Ltd, Germany). Phase correction on the spectra was done manually and automatic adjustment of the baseline was carried out with the help of a polynomial fit with a degree of 3. The spectra were binned at intervals of 0.04 ppm for the chemical shift range of 0.2–10 ppm, omitting the region containing residual water and ethanol [15].

2.4.3. Fourier transforms infrared spectroscopy (FT-IR)

FT-IR spectra were obtained using an FT-IR spectrometer (Thermo Nicolet Nexus 470; Scotia, New York, United States) recorded between 4000 and 400 cm^{-1}, with an optical resolution of 4 cm^{-1}. In brief, 1 mg of sample was grounded with 100 mg of KBr powder using a mortar and pestle. The sample-salt combination was placed into the die chamber, and the plunger was inserted. The O-ring was then fitted over the plunger and a 10-ton load was applied to the die to produce a pellet. Place the FT-IR pellet onto the sample holder of the FT-IR spectrometer, ensuring it is securely positioned and the beam will start to run. Results were analysed using Omnic E.S.P. Software, Version 5.2 (Thermo Fisher Scientific, United States).

2.4.4. X-ray diffraction (XRD) analysis

Crystallinity of the powders was studied using a BRUKER D8 Advance X-ray diffractometer (Bruker AXS GmbH, Karlsruhe, Germany). The powder samples were spread onto a plane quartz glass sample slide and the slide was placed in the X-ray diffractometer. The analysis was performed using the following settings: 40 kV of voltage, 40 mA of current, 2θ scan method (10–50°), 0.1 s of time constant, and 0.02° of angular step. The scan rate was 10° per minute.

2.4.5. Dynamic scanning calorimeter (DSC)

A differential scanning calorimeter (Shimadzu DSC-60, Shimadzu, Tokyo) was used to analyse the thermal properties of the powders in triplicate. Precisely 5 mg of powder was weighed in the aluminium sample pan and sealed hermetically sealed. After 15 min of acclimatisation at room temperature, each sample was heated from 30 to 300 °C at a rate of 10 °C per min. The analysis was performed under nitrogen atmosphere. Analysis of the data was performed using the LabSolutions TA software (Shimadzu, Tokyo).

2.4.6. Thermogravimetric analysis (TGA)

TGA was performed with the use of a thermal analysis apparatus TG/DTA6300 (SII Nano Technology Inc., Tokyo, Japan). Approximately 5 mg of samples were placed onto aluminium pans and were subjected to heating over a range of 30–350 °C, at a rate of 10 °C per minute.

2.4.7. Determination of bulk and tapped density

The powder's bulk and tapped density were estimated using a previously established method [16]. Freshly prepared powders (2 g) were filled into a 10 ml measuring cylinder and its volume was recorded. The formulas for calculating bulk density and tapped density are as follows:

Bulk Density = Mass of Powder / Bulk Volume of Powder

Tapped Density = Mass of Powder / Tapped Volume of Powder

2.4.8. Flowability and cohesiveness

Carr's index (CI) and Hausner's ratio (HR) are commonly used to assess powder's flowability and cohesiveness, respectively. The CI was determined as:

$$\text{Carr's index} = \frac{(\text{tapped density} - \text{bulk density})}{\text{tapped density}} \text{ x } 100.$$

Husner ratio defines powder mixture's flowability and the value indicates the ratio between the bulk and tapped densities.

$$\text{Husner ratio} = \frac{\text{bulk density}}{\text{tapped density}}$$

A Hausner ratio that is higher than 1.22 or a Carr index that is higher than 0.18 indicate poor flowability, whereas a Hausner ratio that is lower than 1.18 or a Carr index that is lower than 0.15 is considered to have acceptable flowability [17].

2.4.9. Angle of repose

The angle of repose was performed following the European Pharmacopeia [18]. A glass plate was put on the table after affixing a funnel to it. To keep the funnel upright, the vertical space between the end of the funnel and the glass was kept at 2 cm. The powder cone was formed by pouring 2 g of powder via the glass funnel vertically on the glass plate. The angle between the conical surface and the horizontal plane was then measured. The powder's angle of repose was calculated using following equation:

$$\text{Tan } \theta = \frac{height}{radius}$$

2.4.10. Dissolution profile

The dissolution profile of the formulations was studied using the Franz diffusion cells (3 cells) system (Heto HMT-200) with phosphate-buffered saline (PBS; pH 7.4) containing 2 % v/v tween 80 as a dissolution medium [19]. Each cell reservoir was filled with 5 mL of PBS and equipped with a magnetic stirrer. The cells were linked to a water bath to keep the temperature of the dissolution media at 37 °C ± 0.5 °C. The experiment under a sink condition.

1 mg of the powder was weighed and deposited on the top compartment of the Franz-cell reservoir, which was covered with a cellulose filter paper (Whatman® qualitative filter paper Grade 5). At predefined time intervals (15, 30, 45, 60, 90, 120, 180, 240, 300, 360, 420, 480, and 540 min), samples were taken from the receptor chamber via the sampling port and replaced with an equal volume of fresh dissolution medium to maintain the sink condition. At the end of the experiment, the filter paper was removed and carefully washed with 2 mL of fresh medium. The amount of drug collected from the filter paper and the receptor chamber were quantified using HPLC. Each formulation was evaluated in triplicate (n = 3) and the dissolution data were represented as a percentage of the drug mass in the sampled solution relative to the total mass of drug recovered.

2.4.11. In vitro aerosol performance of the powders

In vitro aerodynamic performance of the powders was analysed using a Next Generation Impactor (NGI) (Copley, UK) operated according to Pharmacopeia standard at 4 kPa pressure drop with 4 L inhaled air [20]. Each formulation was tested in triplicate using ethanol as a rinsing solvent.

The NGI stages were sprayed with silicone solution prior to the dispersion test. An amount of 10 ± 0.2 mg of powder was filled inside a size 3 HPMC capsule (Alice Li's Pharmaceutical, China). The drug-filled capsule was loaded into a Breezehaler® (Plastiape, Italy) and actuated for 2.4 s at a flow rate of 100 L/min (Copley DFM 2000, UK). The throat was rinsed with 3 mL ethanol, while the capsule, mouth adapter, device and all stages were rinsed with 2 mL ethanol. The amount of drug in each sample solution was quantified using HPLC.

The total fine particle fraction (FPF$_{total}$) was defined as the percentage of the aerosol particles with an aerodynamic diameter less than 5 μm relative to the total recovered drug mass. The emitted fine particle fraction (FPF$_{emitted}$) was characterised by the mass percentage of particles with an aerodynamic diameter less than 5 μm relative to the total recovered drug mass, excluding the capsule and device. The mass median aerodynamic (MMAD) was calculated from the log probability plot of the NGI data. Geometric standard deviation (GSD) was calculated using the same plot as follows:

$$\text{GSD} = (d_{84.13}/d_{15.87})^{1/2}$$

2.4.12. Assessment of cell viability

The A549 cells were seeded at 9×10^3 cells/well in a 96-well plate and incubated at 37 °C in a humidified atmosphere of 10 % CO$_2$ for 24 h. The cells were incubated for 4 h prior to the treatment with different concentrations of andrographolide. Treatment with media was used as a negative control. The cells were incubated with the treatments for 48 h prior to the MTT assay. After incubation, the medium in each well was replaced with MTT solution (0.5 mg/mL) followed by an additional incubation at 37 °C for 4 h. Then, the MTT solution was removed and replaced with 50 μL of DMSO to solubilise the formazan crystals and the absorbance was measured at 560 nm using Varioskan Flash Multimode Reader (Thermo Fisher Scientific, USA). The percentage of cell viability was estimated from

the ratio of absorbance in the wells containing cells treated with andrographolide to absorbance in the wells containing cells treated with media. The percentage of cell viability was calculated using following equation:

Cell viability (%) = [Abs sample / Abs untreated control] × 100

2.4.13. Storage stability of the formulations

The stability of the powders was evaluated under two different conditions for 6 months: (i) 0 % relative humidity (RH), $30 \pm 2\,°C$, and (ii) 65 ± 5 % RH, $30 \pm 2\,°C$. The $30 \pm 2\,°C$ at 65 ± 5 % RH was done according to the intermediate condition following the ICH guideline [21] which represents the storage condition outside the packaging material. Stability condition of $30 \pm 2\,°C$ at 0 % RH was carried out to imitate the dosage form in the blister packaging (0 % RH).

Prior to the testing, ~10 mg of powders were filled in size 3 HPMC capsules. For condition (i), the capsules were stored with silica gel desiccant beads in a vacuum desiccator jar and placed in an oven at a temperature of $30 \pm 3\,°C$. Separately, another batch of capsules was stored in a climate-controlled cabinet (Stability Chamber Binder KBF 240, Binder GmbH, Tuttlingen, Germany) for condition (ii).

2.4.14. Quantification of andrographolide

Andrographolide in all samples was quantified using a HPLC system (LC-20AD, Shimadzu, Kyoto, Japan) fitted with a Phenomenex Luna® 5 μm C18 (250 × 4.6 mm) column as a stationary phase (Torrance, CA 90501 USA). The mobile phase was composed of acetonitrile and water at 30:70 (% v/v) ratio with a flow rate of 1 mL per min and injection volume of 10 μL. The temperature of the column oven (CTO-10AS Shimadzu, Kyoto, Japan) was kept at 30 °C, and the wavelength of the UV detector (SPD-20A Shimadzu, Kyoto, Japan) was 230 nm. The running time was 9 min with retention time of andrographolide at 2.8 min, limit of detection (LOD) of 2 μg/ml and limit of quantification (LOQ) of 6 μg/ml.

2.4.15. Statistical analysis

All data and results are demonstrated as mean ± standard deviation (SD) with n = 3. The student t-test (Microsoft Office Excel, 2017) was used and the probability (*p*) value less than 0.05 were considered as significant.

3. Results

3.1. Particle morphology

The scanning electron micrographs of all samples are shown in Fig. 1 (A-C). The raw andrographolide consisted of large crystals with sizes ranging between 80 and 200 μm. Formulation 1 powder was in the form of more uniformly elongated crystals with a size of 1–6 μm, while smooth spherical particles were observed in Formulation 2 with a size within 1–5 μm.

3.2. Nuclear magnetic resonance (1^H NMR and 13^C NMR analysis)

The nuclear magnetic resonance (NMR) spectrums of raw andrographolide showed several characteristic peaks that correspond to different nuclei in the molecule. The 1^H NMR spectrums (Fig. 2 (A-C)) of raw andrographolide, Formulation 1 and Formulation 2 shows signals in the aromatic region between 7.1 and 8.1 ppm, which can be attributed to the ten aromatic protons in the molecule. The methylene protons appear as multiplets between 3.8 and 4.1 ppm. The 13^C NMR spectrum (Fig. 3 (A-C)) of raw andrographolide, Formulation 1 and Formulation 2 shows a peak at 204.8 ppm corresponding to the carbonyl carbon, as well as several peaks in the oxygenated carbon region between 92.1 and 101.9 ppm. The methylene carbons appear between 34.8 and 36.1 ppm, while the methyl carbon appears at 17.9 ppm. The aromatic carbons appear between 123.5 and 139.8 ppm. In comparison for both formulations, the spectra concluded the absence of significant chemical shift for both 1H and 13C NMR spectrogram.
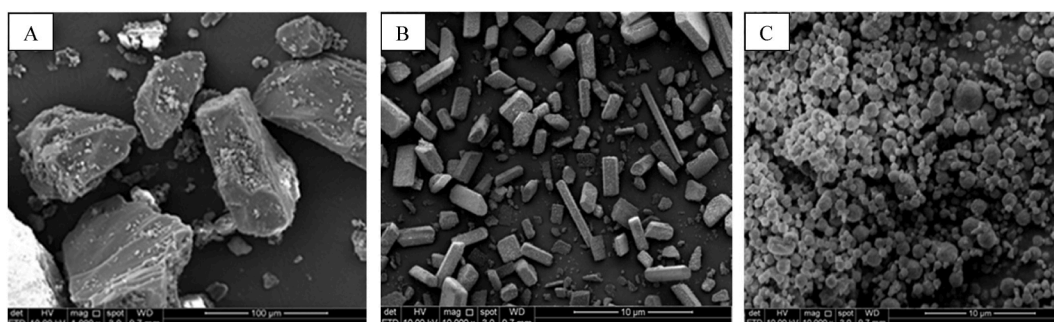

Fig. 1. Scanning electron micrographs of (A) raw andrographolide, (B) Formulation 1 and (C) Formulation 2.

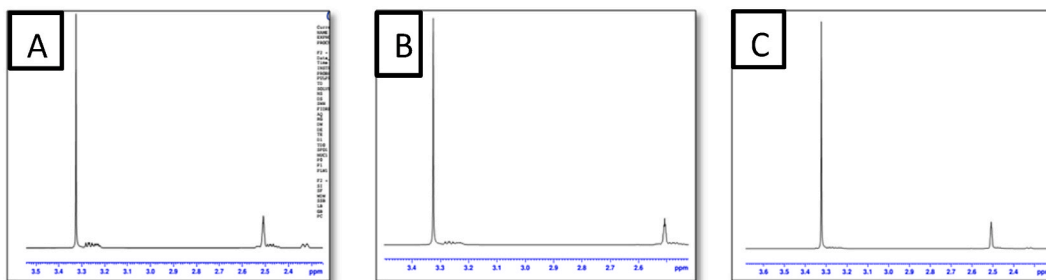**Fig. 2.** [1] H NMR of (A) Raw andrographolide, (B) Formulation 1, (C) Formulation 2.

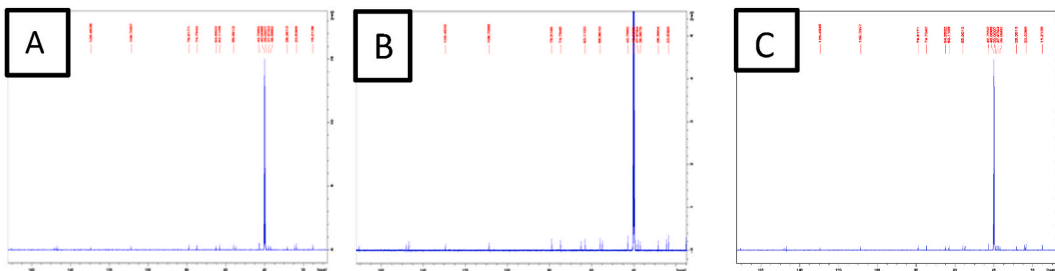**Fig. 3.** ^{13}C NMR of (A) Raw andrographolide, (B) Formulation 1, (C) Formulation 2.

3.3. Fourier-transform infrared spectroscopy (FT-IR)

All three compounds have similar FT-IR spectra without major changes observed (Fig. 4). The raw andrographolide, Formulation 1, and Formulation 2 showed peaks in the range of 3400 and 500 cm^{-1}. The peak at 3100–3500, 2800–3000, 1727, 1458, and 1220 cm^{-1} were andrographolide's O–H, C–H, C=O, C=C and C–O stretching that were generated by the lactone ring's, respectively. A broader peak at 3397.99 cm^{-1} was due to –OH stretching frequency that has been observed for andrographolide. A peak near 2920 cm^{-1} indicated the presence of –COO and a peak which indicated the presence of -O- stretch was seen near 1118.40 cm^{-1}.

3.4. X-ray diffractogram (XRD)

XRD spectra of raw andrographolide, Formulation 1 and Formulation 2 are shown in Fig. 5. Raw andrographolide showed plenty of sharp peaks including the peaks at 10.16°, 12.31°, 18.81°, 22.94°, 27.05°, 29.42° and 31.59°, indicating a typical crystalline structure as reported in the literatures [22,23]. Formulation 1 exhibited similar diffraction peaks as raw andrographolide but with lower intensity, suggesting the inhalable powders are in crystal form. In contrast, Formulation 2 showed broad and diffused peaks with lower intensity indicating the amorphous nature of the powder.
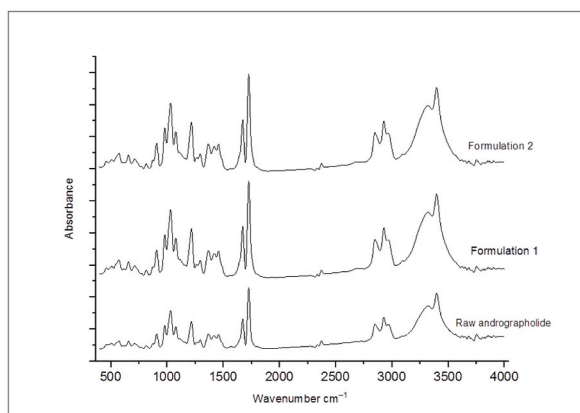

Fig. 4. FT-IR spectra of raw andrographolide, Formulation 1 and Formulation 2.
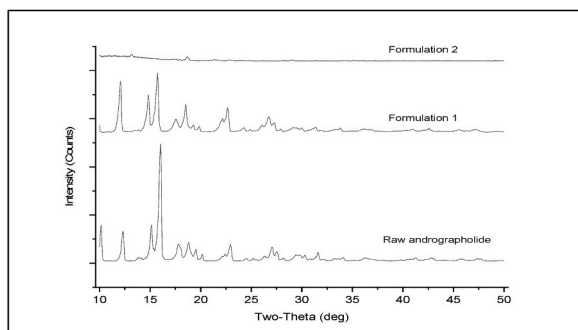
Fig. 5. XRD spectra of raw andrographolide, Formulation 1 and Formulation 2.

3.4.1. Differential scanning calorimetry (DSC)

Fig. 6 showed the DSC thermogram of all samples. Raw andrographolide, Formulation 1 and Formulation 2 showed a sharp endothermic peak, which corresponded to their melting temperature at 230.29 ± 0.21 °C, 229.34 ± 2.77 °C, 229.97 ± 4.41 °C, respectively (n = 3). The melting temperatures suggest no major changes in the thermal properties of both formulations compared to the raw andrographolide.

3.5. Thermogravimetric analysis (TGA)

Fig. 7 displays the TGA thermogram of raw andrographolide, Formulation 1 and Formulation 2. Both formulations showed moisture content of between 0.67-0.93 % and 0.93–3.56 %, respectively which was observed from the minimal drop in the weight of the samples between 80 and 120 °C heating.

3.6. Evaluation of the powder properties

Powder properties of all formulations were compared to the raw andrographolide in Table 1. Formulation 1 showed the lowest angle of repose (28.61°), whereas raw andrographolide showed the highest angle of repose (31.93°). Formulation 1 also showed the best flowability (Hausner ratio of 1.08 and Carr's Index of 13.65 ± 1.04) followed by Formulation 2 (Hausner ratio of 1.25 and Carr's Index of 20.67 ± 2.3) and raw andrographolide (Hausner ratio of 1.47 and Carr's Index of 31.67 ± 1.53). The bulk densities of the powders were between 0.67 and 0.68 g/ml.

3.7. Dissolution profile

Fig. 8 shows the dissolution profile of both formulations in PBS pH 7.4. Formulation 1 and 2 were able to dissolve up to 8.24 % ± 0.34 and 10.59 % ± 0.21, respectively in 9 h. The results showed that the rate at which formulation 2 dissolves is slightly higher than that of formulation 2.

3.8. In vitro aerosol deposition study

Both formulations displayed acceptable FPF_{total} and $FPF_{emitted}$ for pulmonary delivery in the range of 39.29–46.20 % and
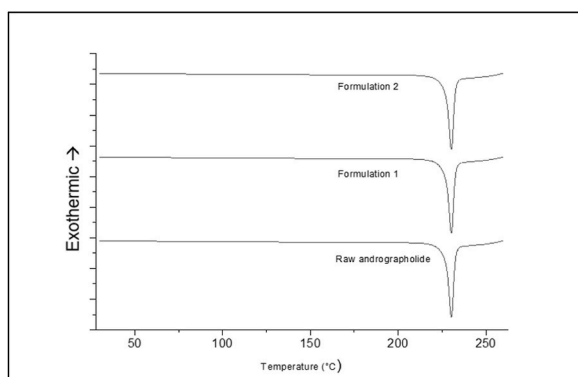

Fig. 6. Dynamic scanning calorimetry thermograms of raw andrographolide, Formulation 1 and Formulation 2.
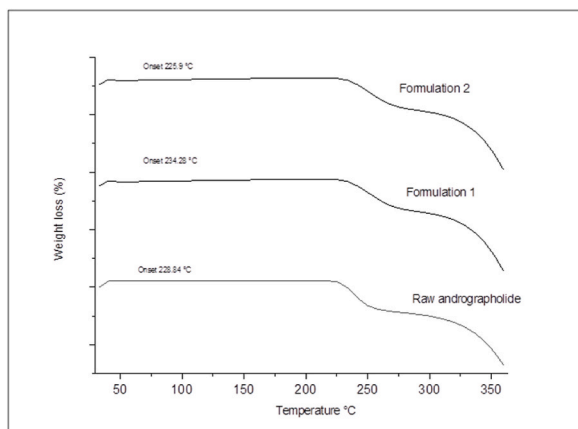
Fig. 7. Thermogravimetric analysis thermogram of raw andrographolide, Formulation 1 and Formulation 2.

Table 1
Powder properties of all Formulation 1 and Formulation 2 compared to the raw andrographolide. Mean ± SD, n = 3.

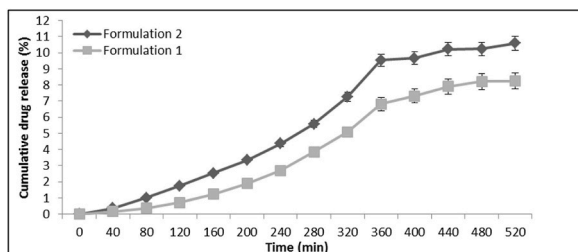|	Raw Andrographolide	Formulation 1	Formulation 2
Angle of repose [θ]	31.93 ± 0.86	28.61 ± 0.38	29.96 ± 0.23
Bulk density [g/ml]	0.67 ± 0.00	0.68 ± 0.01	0.67 ± 0.00
Tapped density [g/ml]	0.97 ± 0.03	0.74 ± 0.03	0.89 ± 0.02
Husner ratio	1.47 ± 0.03	1.08 ± 0.03	1.25 ± 0.03
Carr's index [%]	31.67 ± 1.53	13.65 ± 1.04	20.67 ± 2.3

Fig. 8. Release profiles of andrographolide from Formulation 1 and Formulation 2 using Franz cell dissolution apparatus over a period of 9 h. Mean ± SD, n = 3.

Table 2
Aerosolisation properties of formulations containing andrographolide during the 6 month stability study. Mean ± SD, n = 3.

	30 °C, 0 % Relative humidity							
	Formulation 1				Formulation 2			
Month	0	1	3	6	0	1	3	6
FPF_{total} (%)	43.58 ± 2.50	42.99 ± 3.27	39.51 ± 1.27	40.68 ± 1.30	42.79 ± 3.50	41.89 ± 1.45	42.40 ± 3.00	[a]36.90 ± 0.76
$FPF_{emitted}$ (%)	44.36 ± 2.49	41.82 ± 3.61	40.42 ± 1.47	40.85 ± 1.66	44.78 ± 3.22	43.22 ± 1.80	44.20 ± 2.95	[a]38.20 ± 1.08
MMAD (μm)	5.27 ± 0.12	5.35 ± 0.22	5.58 ± 0.03	5.44 ± 0.10	5.51 ± 0.25	5.35 ± 0.05	5.59 ± 0.23	[a]5.85 ± 0.12
GSD	1.22 ± 0.03	1.21 ± 0.05	1.32 ± 0.02	1.15 ± 0.02	1.30 ± 0.21	1.17 ± 0.02	1.17 ± 0.10	1.27 ± 0.10
	30°C, 65 % Relative humidity							
	Formulation 1				Formulation 2			
Month	0	1	3	6	0	1	3	6
FPF_{total} (%)	43.58 ± 2.50	40.25 ± 1.61	39.16 ± 4.32	41.27 ± 0.10	42.79 ± 3.50	[a]38.94 ± 1.39	[a]37.13 ± 4.02	[a]36.90 ± 1.37
$FPF_{emitted}$ (%)	44.36 ± 2.49	40.68 ± 1.46	40.69 ± 0.91	41.87 ± 0.11	44.78 ± 3.22	[a]39.92 ± 1.52	[a]39.09 ± 3.37	[a]37.43 ± 1.38
MMAD (μm)	5.27 ± 0.12	5.44 ± 0.09	5.58 ± 0.49	5.38 ± 0.10	5.51 ± 0.25	[a]5.61 ± 0.09	[a]5.81 ± 0.71	[a]5.71 ± 0.07
GSD	1.22 ± 0.03	1.16 ± 0.01	1.66 ± 0.21	1.14 ± 0.01	1.30 ± 0.21	1.25 ± 0.01	1.34 ± 0.01	[a]1.18 ± 0.01

[a] *p* values < 0.05 were considered significant differences compared to the 0 month.

42.87–48.00 %, respectively (Table 2). It should be noted that both formulations showed a larger deposition of drugs in stage 1 and 2 (Fig. 9). Formulation 2 showed a higher deposition at stage 4–6 compared to Formulation 1, due to the smaller particle size of amorphous andrographolide particles compared to the crystalline counterpart. The MMAD of both formulations were about 5.15–5.76 μm, while the GSD was less than 1.3.

4. Storage stability studies

Both formulations were stored in two different storage conditions: 30 °C, 0 % RH and 30 °C, 65 % RH. Formulation 1 showed no significant changes in FPF_{total}, $FPF_{emitted}$ and MMAD up to 6 months ($p > 0.05$) in both storage conditions. In comparison, Formulation 2 displayed a significant reduction in FPF_{total}, $FPF_{emitted}$ and MMAD in the sixth month at 30 °C, 0 % RH storage. Further evaluation of Formulation 2 at 30 °C, 65 % RH showed a significant reduction ($p < 0.05$) of $FPF_{total,}$ $FPF_{emitted}$ and MMAD from the first month onwards.

5. *In vitro* cytotoxicity study

As shown in Table 3, raw andrographolide and Formulation 1 showed an IC_{25} value higher than Formulation 2 when tested against A549 cell line, suggesting Formulation 2 has superior anti-cancer activity as compared to Formulation 1 and raw andrographolide.

6. Discussions

In the present study, two formulations containing andrographolide were produced and characterised. Formulation 1 was prepared by dissolving andrographolide in ethanol–water cosolvent system, followed by the application of heat to evaporate the ethanol and precipitate the andrographolide crystals in the water phase. The resulted suspension was homogenised and spray dried. On the other hand, Formulation 2 was produced by direct spray drying of andrographolide in ethanol–water cosolvent system. Spray drying produces small size particles due to the atomisation of a liquid feed into fine droplets, which increases the surface area for rapid evaporation of solvent or carrier liquid. The hot air used in the spray drying process further promotes fast evaporation of the solvent or carrier liquid from the droplets, resulting in the formation of solid particles [24].

Both Formulation 1 and Formulation 2 have similar physicochemical (except morphology and crystallinity) properties as the raw unprocessed andrographolide, suggesting both formulations are suitable for preclinical and clinical trials. SEM images (Fig. 1) revealed that Formulation 1 was long and thin-shaped crystals while Formulation 2 was spherical particles.

Comparing the NMR spectra of crystalline and amorphous andrographolide can provide insights into the molecular arrangement and structural characteristics of the compound in its different forms. NMR spectra of Formulation 1 and Formulation 2 exhibit distinct peaks corresponding to different protons and carbon atoms in the molecule which were identical to raw andrographolide (Figs. 2 and 3). This suggests that both formulations contain andrographolide and have no impurities. On the other hand, by analyzing the FT-IR spectra of Formulation 1 and 2, we can gain valuable information about the structural characteristics and solid-state properties of the compound, which can be useful for formulation development, stability studies, and understanding its behaviour in different environments [25]. As described above (Fig. 4), all three formulations had similar spectra indicating most of the chemical bond was retained even after formulation. In addition, NMR and FT-IR spectra showed no ethanol chemical shift in both formulations, indicating they were free of organic solvent and suitable for pulmonary drug delivery.

The presence of sharp, well-defined diffraction peaks in the XRD pattern indicates a crystalline structure, while a broad hump or absence of peaks (halo pattern) suggests an amorphous structure. The raw andrographolide was crystals in nature and it was reconfirmed using XRD which revealed multiple peak diffractions as the previously published article [22,26]. This was further investigated for Formulation 1, which also showed a similar crystalline pattern as the raw andrographolide. In contrast, Formulation 2 did not have any well-defined peaks suggesting it was amorphous in nature.

Thermal behaviour, melting point, phase transitions, and stability of pharmaceutical compounds were evaluated using DSC, while weight changes of a sample as a function of temperature were done by using TGA. DSC profiles suggest the melting point of both formulations was similar to the raw andrographolide. There were no changes in melting point and thermal behaviour for both formulations. TGA profiles reveal moisture content was within the 5 % range for both formulations which is usually suitable for pharmaceutical applications [27].

The flow properties of the medication are important considerations in pharmaceutical formulation and processing. However, specific information about the flow properties of andrographolide may be limited. Based on our experimental data, Formulation 1, consisting of well-defined crystals showed better flow properties compared to raw andrographolide and Formulation 2. This was supported by Hausner's ratio and Carr index values of Formulation 1 that were within the standard reference values which are below 1.18 and 15, respectively [17].

The rate and extent of drug release for andrographolide was evaluated using a Franz cell system. The dissolution profile of Formulations 1 and Formulation 2 showed a maximum drug release of 8.24 % and 10.59 %, respectively, in 9 h. This suggests that the particles may not undergo rapid solubilisation upon deposition in the lungs. This can be advantageous for lung cancer treatment as the patients may not need to receive frequent dosing, which could enhance patient compliance towards the treatment. However, prolonged drug retention in the lung surface may elicit hypersensitivity reactions which require further evaluation. On the other hand, Zhang et al. (2016) [22] reported more than 50 % andrographolide release within 5 min as compared to less than 11 % drug release up to 9 h in the current study. This could be due to: (i) the incorporation of porous silicon dioxide in their formulation to increase the
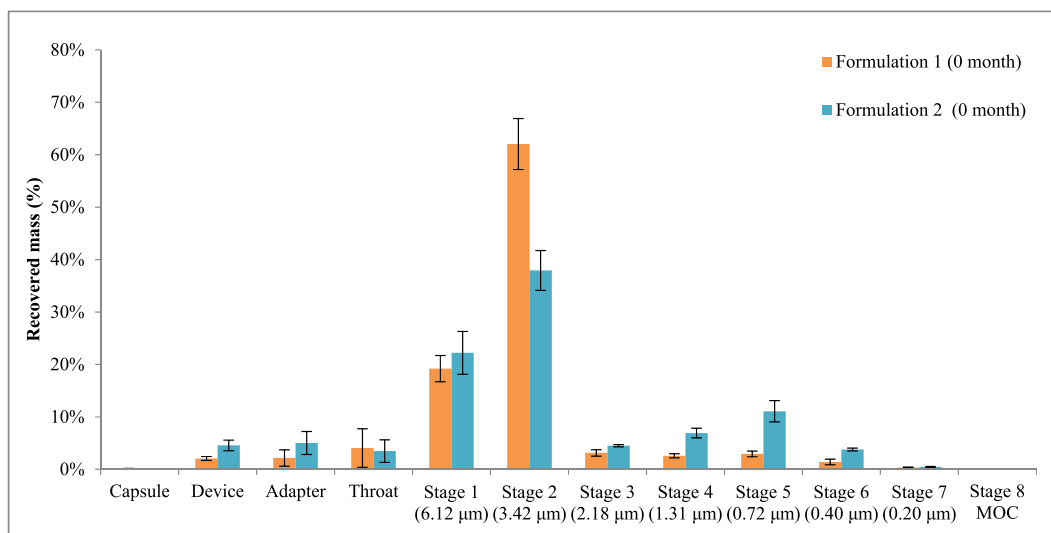
Fig. 9. Dispersion profiles of Formulation 1 and Formulation 2 at 100 L/min for 2.4sec using a Breezehaler at 0 month.

Table 3

Inhibitory cytotoxic concentration of raw andrographolide, Formulation 1 and Formulation 2 on human alveolar basal carcinoma epithelial (A549) cell lines.

Compound/Formulation	Inhibitory cytotoxic concentration (μg/mL)	
	IC_{25}	IC_{50}
Raw andrographolide	29.75 ± 3.10	117.02 ± 13.2
Formulation 1	31.91 ± 1.81	163.39 ± 13.5
Formulation 2	6.57 ± 1.08	>200

specific surface area, which led to a faster drug release, and (ii) Zhang et al. (2016) [22] utilised a paddle dissolution apparatus, which employs a rotating paddle for uniform mixing within the dissolution medium and promoting faster dissolution rates by enhancing mass transfer and reducing diffusion limitations. However, the paddle apparatus was not utilised in this study as the well-stirred environment may contrast with the *in vivo* condition of the alveolar regions in the lung [28]. While the static system of the Franz cell in this study may have led to slower dissolution kinetics in our study, it may better simulate the conditions of drug release in the lung.

Both crystalline and amorphous powders were found to be with an FPF_{total} of more than 40 %. However, Formulation 1 with elongated crystal structures showed slightly enhanced aerosolisation properties as compared to the spherical amorphous structures of Formulation 2, with slightly higher FPF ($p > 0.05$). The elongated nature of the andrographolide crystals prevents close packing of particles, thereby substantially reducing cohesiveness between particles via van der Waals forces [29]. In contrast, the spray-dried amorphous andrographolide particles showed spherical morphologies with a tendency to agglomerate [30]. For both formulations highest deposition was observed in stages 1 and 2, representing particles with aerodynamic diameters of <6.12 μm and <3.42 μm, respectively. However, the elongated morphology of the crystalline powder (Formulation 1) gave slightly more favourable *in vitro* aerosol deposition in stages 1 and 2 when compared to the amorphous andrographolide (Formulation 2). The elongated andrographolide crystals are expected to deposit deep in the lungs via interception. In contrast, spray-dried amorphous andrographolide particles showed spherical morphologies with a tendency to agglomerate and may deposit in the lungs via inertial impaction and sedimentation [31].

Andrographolide stability has been a subject of research due to its pharmaceutical importance. Several studies have investigated the factors affecting its stability and degradation pathways [12]. Andrographolide degraded at high storage temperatures and the degree of degradation increased with temperature. However, at lower storage temperatures, such as 5–30 °C, there was no discernible loss of andrographolide during the course of the research [12,32]. In our study, Formulation 1 was stable which was portrayed via insignificant changes in FPF_{total}, $FPF_{emitted}$, MMAD and GSD upon storage up to 6 months ($p > 0.05$) at 30 °C, 0 % RH and 30 °C, 65 % RH. When Formulation 1 was viewed under SEM, no morphological changes were observed, suggesting the particles were still intact for up to 6 months. On the other hand, the particles in the Formulation 2 tend to fuse together as observed under SEM when stored at 65 % RH for 6 months (Supplementary data). No chemical degradation was observed in both formulations at both conditions for up to 6 months which was measured via XRD and FT-IR. These findings underscore the need for further investigations.

In this work, we determined the cytotoxicity of andrographolide by treating A549 cells (10^5 cells/ml) with various concentrations of andrographolide for 24 h followed by MTT assay. Raw andrographolide and Formulation 1 had almost similar IC_{25} values of 29.75 $\pm$ 3.10 and 31.91 $\pm$ 1.81, respectively. Formulation 2 showed a lower IC_{25} value of 6.57 $\pm$ 1.08. Hence, the amorphous

andrographolide had a higher cytotoxic effect on cancer cells compared to the crystalline form. The enhanced anti-cancer activity of Formulation 2 could be due to increased andrographolide solubility in the cell culture media compared to Formulation 1. The increased solubility could be primarily due to the higher molecular mobility in amorphous solids of Formulation 2. While the arrangement of molecules is highly ordered and regular in crystalline solids of Formulation 1, which can restrict the movement of water molecules and hinder the solubility. Amorphous solids lack this long-range order and have a more disordered molecular structure. This increased disorder allows for greater molecular mobility and facilitates the interaction of the solid molecules with the water molecules, leading to enhanced solubility.

7. Conclusions

In conclusion, two (2) novel inhalable formulations of andrographolide composed of crystals and amorphous particles were prepared with good aerosol performance and promising anti-cancer properties. Production of these formulations used simple precipitation and spray drying techniques which are robust and easily scalable for large manufacturing. Dry powder formulations of andrographolide show great promise for pulmonary drug delivery. The physicochemical properties of andrographolide, such as its low solubility and high melting point present challenges in formulation development, but these can be overcome through the use of appropriate processing techniques. Moreover, *in vitro* studies have shown that andrographolide can induce apoptosis in cancer cells, making it a promising candidate for the treatment of lung cancer. Overall, the development of dry powder formulations of andrographolide for pulmonary drug delivery has the potential to offer an effective and safe treatment option for patients with pulmonary diseases. However, further research is needed to fully understand the pharmacokinetics and pharmacodynamics of this drug in the lung and to translate these findings to clinical applications.

CRediT authorship contribution statement

Shankar Jothi: Methodology, Investigation, Conceptualization. **Noratiqah Mohtar:** Writing – review & editing. **Mas Jaffri Masarudin:** Supervision, Resources. **Thaigarajan Parumasivam:** Writing – review & editing, Supervision, Resources.

Declaration of competing interest

The authors declare that they have no known competing financial interests or personal relationships that could have appeared to influence the work reported in this paper.

Appendix A. Supplementary data

Supplementary data to this article can be found online at https://doi.org/10.1016/j.heliyon.2024.e30761.

References

[1] American Cancer Society, Cancer Facts & Figures 2021, American Cancer Society, Atlanta, 2021. https://www.cancer.org/content/dam/cancer-org/research/cancer-facts-and-statistics/annual-cancer-facts-and-figures/2021/cancer-facts-and-figures-2021.pdf.
[2] National Cancer Institute, Chemotherapy Side Effects, 2021. https://www.cancer.gov/about-cancer/treatment/types/chemotherapy/side-effects.
[3] G. Liu, H. Chu, Andrographolide inhibits proliferation and induces cell cycle arrest and apoptosis in human melanoma cells, Oncol. Lett. 15 (2018) 5301–5305.
[4] K. Sheeja, et al., Antiangiogenic activity of *Andrographis paniculata* extract and andrographolide, Int. Immunopharm. 7 (2007) 211–221.
[5] J.H. Lee, et al., Dietary phytochemicals and cancer prevention: Nrf2 signaling, epigenetics, and cell death mechanisms in blocking cancer initiation and progression, Pharmacol. Therapeut. 137 (2013) 153–171.
[6] Z. Chen, et al., Andrographolide inhibits non-small cell lung cancer cell proliferation through the activation of the mitochondrial apoptosis pathway and by reprogramming host glucose metabolism, Ann. Transl. Med. 9 (2021) 1701.
[7] J.P. Loureiro Damasceno, et al., *Andrographis paniculata* formulations: impact on diterpene lactone oral bioavailability, Eur. J. Drug Metabol. Pharmacokinet. 47 (2022) 19–30.
[8] P. Songvut, et al., Comparative pharmacokinetics and safety evaluation of high dosage regimens of *Andrographis paniculata* aqueous extract after single and multiple oral administration in healthy participants, Front. Pharmacol. 14 (2023) 1230401.
[9] A. Kaewdech, et al., The use of *Andrographis paniculata* and its effects on liver biochemistry of patients with gastrointestinal problems in Thailand during the COVID-19 pandemic: a cross sectional study, Sci. Rep. 12 (2022) 18213.
[10] X. Zhang, et al., Influence of andrographolide on the pharmacokinetics of warfarin in rats, Pharmaceut. Biol. 56 (2018) 351–356.

[11] A. Balap, et al., Pharmacokinetic and pharmacodynamic herb-drug interaction of *Andrographis paniculata* (Nees) extract and andrographolide with etoricoxib after oral administration in rats, J. Ethnopharmacol. 183 (2016) 9–17.

[12] P. Phattanawasin, et al., Isolation and characterization of the acid and base degradation products of andrographolide, Pharmazie 73 (2018) 559–562.

[13] Y. Yan, et al., Andrographolide, Nat. Small Molecule Drugs from Plants 1 (2018) 357–362.

[14] N. Alhajj, et al., Designing enhanced spray dried particles for inhalation: a review of the impact of excipients and processing parameters on particle properties, Powder Technol. 384 (2021) 313–331.

[15] A.A.I. Alapid, et al., Investigation of andrographolide effect on non-infected red blood cells using the (1)H-NMR-based metabolomics approach, Metabolites 11 (2021).

[16] United States Pharmacopeia, General Chapter <616> Bulk Density and Tapped Density of Powders, in: United States Pharmacopeia and National Formulary (USP 43-NF 38), 2020.

[17] T. Hao, Understanding empirical powder flowability criteria scaled by Hausner ratio or Carr index with the analogous viscosity concept, RSC Adv. 5 (2015) 57212–57215.

[18] European Pharmacopoeia, Powder Flow, 2008.

[19] Y.-J. Son, et al., Optimization of an in vitro dissolution test method for inhalation formulations, Dissolution Technol. 17 (2010) 6–13.

[20] United States Pharmacopeia, USP37-NF 30, in: Chapter 601: Physical Tests and Determinations; Aerosols, 2021. http://www.uspbpep.com/usp31/v31261/usp31nf26s1_c601.asp.

[21] ICH Harmonised Tripartite Guideline, Q1A(R2) Stability Testing of New Drug Substances and Products, 2003. https://database.ich.org/sites/default/files/Q1A_R2_Guideline.pdf.

[22] D. Zhang, et al., Preparation and evaluation of andrographolide solid dispersion vectored by silicon dioxide, Phcog. Mag. 12 (2016) S245–S252.

[23] G. Zhao, et al., Effect of carrier lipophilicity and preparation method on the properties of andrographolide solid dispersion, Pharmaceutics 11 (2019).

[24] S. Daniel, et al., in: P. Rosario, M. Teresa (Eds.), Spray Drying: an Overview, Biomaterials, IntechOpen, 2017. Ch. 2.

[25] R.M. Silverstein, et al., Spectrometric Identification of Organic Compounds, seventh ed., Wiley, 2005.

[26] P. Imsanguan, et al., A preliminary study of andrographolide precipitation from *Andrographis paniculata* extracts using a supercritical anti-solvent (SAS), Sci. Technol. Aliment. 15 (2015) 76–82.

[27] A. Crouter, L. Briens, The effect of moisture on the flowability of pharmaceutical excipients, AAPS PharmSciTech 15 (2014) 65–74.

[28] B.B. Eedara, et al., Dissolution and absorption of inhaled drug particles in the lungs, Pharmaceutics 14 (2022).

[29] C.D. Reddy, et al., Two-dimensional van der Waals C60 molecular crystal, Sci. Rep. 5 (2015) 12221.

[30] K. Pitt, et al., Particle design via spherical agglomeration: a critical review of controlling parameters, rate processes and modelling, Powder Technol. 326 (2018) 327–343.

[31] N. Shetty, et al., Physical stability of dry powder inhaler formulations, Expet Opin. Drug Deliv. 17 (2020) 77–96.

[32] S.Y. Lee, et al., Stability and toxicity profile of solution enhanced dispersion by supercritical fluids (SEDS) formulated *Andrographis paniculata* extract, Braz. J. Chem. Eng. 36 (2019) 969–978.